



Mobilized Bearing Capacity Analysis of Global Stability for Walls Supported by Aggregate Piers

Daniel R. VandenBerge, P.E., M.ASCE¹; Emily C. Reed²; and Ruidong Li³

Abstract: Global stability analysis is a key component of mechanically stabilized earth (MSE) wall design, especially those constructed over marginal soils. When limit equilibrium analysis is used for MSE wall design, incorrect factors of safety can be predicted depending on the shape assumed for the failure surface. The use of ground improvement, such as aggregate piers (AP), further complicates the analysis. A mobilized bearing capacity (MBC) approach is presented which highlights the direct relationship between the factors of safety for global stability and bearing capacity. Results from the MBC approach are compared with finite element strength reduction analyses for a range of MSE wall geometries and AP replacement ratios. The factors of safety match well for global factors of safety between 1 and 1.5, considering both eccentricity and stress concentration. The MBC approach provides a tool to supplement and refine global stability analyses for retaining walls constructed over improved foundations. DOI: [10.1061/\(ASCE\)GT.1943-5606.0002540](https://doi.org/10.1061/(ASCE)GT.1943-5606.0002540). © 2021 American Society of Civil Engineers.

Introduction

Retaining walls, including mechanically stabilized earth (MSE) walls, are designed for failure modes including sliding, settlement, bearing capacity, and global stability. Whereas it is common to evaluate each of these modes in isolation, the stress-deformation behaviors of the wall, backfill, and foundation soil have a combined impact on the wall's performance in each mode (FHWA 2016). In particular, this paper explores the connection between bearing capacity and global stability to provide insight into the critical global stability mechanisms and to present an alternative approach to limit equilibrium or numerical analysis for evaluating global stability of such structures.

The basic components of an MSE retaining wall cross section are shown on the left side of Fig. 1. The MSE wall retains a backfill zone, and both are supported by a foundation soil (a.k.a., matrix soil), which may include a zone of soil improvement. For global stability analysis of this system, failure surfaces behind the stronger MSE zone will pass through multiple soils, which may be drained, undrained, or a combination of both. The most broadly available and widely practiced, but not necessarily best, method for this type of global stability analysis is limit equilibrium (e.g., Leshchinsky and Han 2004; FHWA 2009; Stuedlein et al. 2010).

A key aspect of evaluating global stability using limit equilibrium is the selection of an appropriate failure surface (or set of surfaces) to analyze. The complexity of the critical failure surface for a retaining wall is illustrated in Fig. 1. The use of rigorous limit equilibrium procedures (e.g., Spencer 1967) with robust search routines will find failure surfaces that balance shear strength with applied

shear stress. The inclination of these surfaces will tend to be statically correct within a given soil zone, particularly when noncircular failure surfaces are allowed. However, a correct failure surface shape also must be physically possible, which is sometimes referred to as kinematic admissibility, and must not imply stress discontinuities in the soil. A classic example of a kinematically admissible surface is a circular arc, which does not require any slippage between adjacent soil zones.

The effect of failure surface shape on limit equilibrium analysis of retaining walls was examined by VandenBerge (2017) for homogenous foundation conditions. As an upper bound solution, circular failure surfaces provide a kinematically admissible shape but tend to overestimate the factor of safety, F . Referring to the left side of Fig. 1, a circle is not the critical shape through the foundation zone and does not correctly match the failure surface through the retained soil. On the other hand, VandenBerge (2017) showed that the use of optimization schemes with noncircular failure surfaces usually leads to a V -shaped surface that is statically, but not kinematically, admissible. In other words, without proper constraints, limit equilibrium analysis will seek out the lowest factor of safety even if the associated failure surface is not physically possible. Sloan (2013) also shows that the correct failure surface shape lies between circular and V -shaped surfaces.

In addition to the correct failure surface shape, limit equilibrium methods require assumptions about the inclination of side forces between slices. For most slopes, the effect of side force inclination on the factor of safety is commonly assumed to be small (Duncan et al. 2014). However, VandenBerge (2017) also showed the important influence of the side force assumptions for cross sections with an abrupt change in load, such as a vertical wall face. The selection of an appropriate side force function for this type of problem is nontrivial.

The difficulties of selecting a correct failure surface shape and side force function are significant limitations for limit equilibrium, which is the most common tool for assessing global stability of retaining walls. To some extent, these difficulties can be bypassed using numerical analysis, such as stress-deformation strength reduction analysis or plasticity-based limit analysis. While attractive for some projects, the time and effort associated with strength reduction analysis are not economically feasible in many cases. Limit analysis is powerful but less widely used at present. As an alternative, VandenBerge (2017) recognized that the retaining wall system could be converted to an analogous strip foundation supporting

¹Assistant Professor, Dept. of Civil and Environmental Engineering, Tennessee Technological Univ., Box 5015, Cookeville, TN 38505 (corresponding author). ORCID: <https://orcid.org/0000-0001-6680-8094>. Email: dvandenberge@tntech.edu

²Project Consultant, Civil & Environmental Consultants, Inc., 117 Seaboard Ln., Suite E-100, Franklin, TN 37067.

³Associate Project Engineer, Geopier Foundation Company, 130 Harbour Place Dr., Suite 220, Davidson, NC 28306.

Note. This manuscript was submitted on November 5, 2019; approved on February 23, 2021; published online on April 8, 2021. Discussion period open until September 8, 2021; separate discussions must be submitted for individual papers. This paper is part of the *Journal of Geotechnical and Geoenvironmental Engineering*, © ASCE, ISSN 1090-0241.

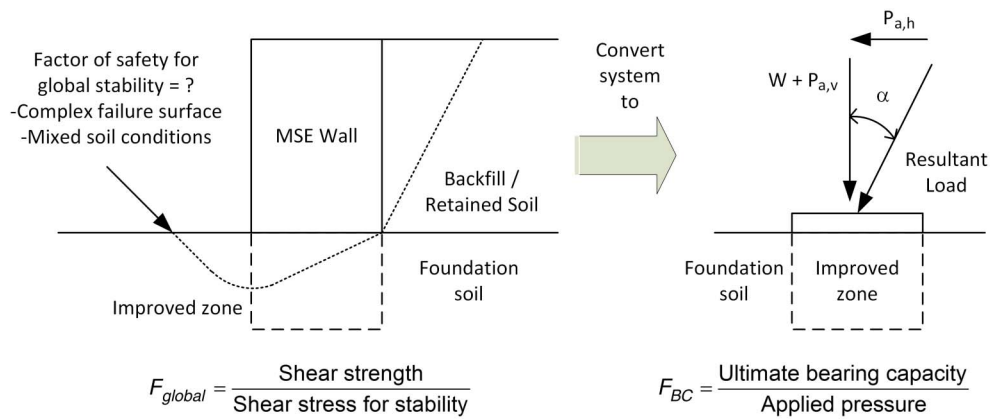


Fig. 1. Global stability of an MSE wall construed as a bearing capacity problem with an inclined load.

an inclined load as shown at the right of Fig. 1. Stability of the analogous foundation can be predicted using bearing capacity theory (e.g., Meyerhof 1963). The advantages of this approach are: (1) it leverages robust plasticity-based bearing capacity solutions, (2) practicing engineers are familiar with these solutions, and (3) the analytical equations can be solved iteratively in a spreadsheet or similar desktop application. Leshchinsky et al. (2012) showed that the equivalent footing approach using Meyerhof (1963) predicted similar bearing capacity to limit analysis and also illustrated that the load inclination cannot be safely ignored.

After reviewing the basics of bearing capacity analysis, this paper will explore the application of bearing capacity theory to global stability assessment of MSE walls through a mobilized shear strength approach that accounts for differences in the definition of the factor of safety. The approach is applied to MSE walls supported by foundations improved using aggregate piers (AP). However, the method can also be used on unimproved foundation soils (VandenBerge 2017). The analytical results are validated using finite element strength reduction analyses, and design recommendations are presented for use of bearing capacity analysis for the global stability of MSE walls supported by improved foundations.

Background

Bearing Capacity Analysis

The mechanics of global stability is closely linked to that of bearing capacity, which is demonstrated by Duncan et al. (2014) for slopes and VandenBerge (2017) for retaining walls. In this study, the Meyerhof's (1963) approach to bearing capacity was chosen as the analytical bearing capacity method. A key feature in Meyerhof's method is the inclusion of load inclination factors in an analytical

form. The Meyerhof method allows for the direct calculation of bearing capacity, depth, and load inclination factors, all of which may be important for retaining walls.

Meyerhof's (1963) bearing capacity factors (N_c , N_q , and N_γ) and correction factors for depth, d , and inclination, i , are summarized in Table 1 for use with the calculation of ultimate bearing capacity, q_{ult} , as:

$$q_{ult} = d_c i_c c' N_c + d_q i_q \gamma D N_q + 0.5 d_\gamma i_\gamma \gamma B' N_\gamma \quad (1)$$

where c' = effective cohesion intercept, γ = soil unit weight, D = foundation depth, and B' = effective foundation width. The bearing capacity factors depend on the effective stress friction angle of the soil, ϕ' , whereas the inclination factors depend also on the load inclination, α . Meyerhof's load inclination factors are empirical corrections based on observations from laboratory scale experiments. For eccentric loading, Meyerhof also suggested a reduced area approach where the foundation load can be practically represented by a uniform stress calculated as:

$$q_{applied} = \frac{N}{B - 2e} = \frac{N}{B'} \quad (2)$$

where N = total vertical load, B = foundation (or wall width), e = eccentricity, and B' = reduced foundation width corrected for eccentric loading.

For undrained conditions, Ukritchon et al. (1998) compared the results of upper and lower bound plasticity-based limit analysis to Meyerhof's solution for combined eccentric and inclined loading. They found that Meyerhof's reduced area approach [Eq. (2)] accounts appropriately for eccentricity over a wide range of e/B ratios without inclined loading. Meyerhof's empirical correction for inclined loading predicted ultimate bearing capacities, q_{ult} , that were about 20%–25% lower than the corresponding limit analyses.

Table 1. Bearing capacity factors and correction terms for strip loading

Factor	N_c term	N_q term	N_γ term
Bearing capacity	$N_c = (N_q - 1) \cot \phi'$	$N_q = e^{\pi \tan \phi'} N_{\phi'}$	$N_\gamma \approx (N_q - 1) \tan(1.4 \phi')$
Depth	$d_c = 1 + 0.2 \sqrt{N_{\phi'}} (D/B)$		For $\phi = 0^\circ$: $d_q = d_\gamma = 1$ For $\phi' > 10^\circ$: $d_q = d_\gamma = 1 + 0.1 \sqrt{N_{\phi'}} (D/B)$
Inclination		$i_c = i_q \approx \left(1 - \frac{\alpha}{90^\circ}\right)^2$	For $\phi' > 0^\circ$: $i_\gamma \approx (1 - \alpha/\phi')^2$ For $\phi = 0^\circ$: $i_\gamma = 0$

Source: Data from Meyerhof (1963).

Note: $N_c = 5.14$ for saturated, undrained conditions ($\phi = 0$), $N_{\phi'} = \tan^2(45 + \phi'/2)$.

Meyerhof's inclination factors result in the highest error when α is high and are not appropriate when α exceeds about 16° for undrained conditions. However, at these high values of α , sliding becomes more critical than bearing capacity and should control design instead of global stability.

Ground Improvement Modeling

Ground improvement is often required to reduce settlement and increase stability in cases where global stability is an important design consideration. Aggregate piers are an efficient means of improving global stability of MSE walls built over soft soils (e.g., Mankbadi et al. 2004; Hutchinson 2011; Diaz et al. 2012). Aggregate piers are installed by drilling a shaft of desired length and then filling the hole with heavily compacted aggregate. This aggregate is placed in lifts and each lift is hydraulically rammed by a beveled tamper. Based on the required capacity of the piers, an area replacement ratio, R_a , is selected, which is equivalent to the ratio of the volume (or area in plan view) of the existing matrix soil that is replaced by the piers to the total volume of the reinforced soil.

Modeling of an AP improved zone is inherently a three-dimensional (3D) problem because of the spacing of the piers. However, it is very common to convert from a 3D plan view to a 2D elevation view, or plane strain condition, for modeling purposes. One method is the equivalent area approach in which the aggregate piers are converted into equivalent panels sized according to the replacement ratio as indicated in Fig. 2. Based on data from a pile-supported embankment, Ariyaratne et al. (2013) found that the 2D equivalent area approach predicted movements similar to those predicted by a corresponding 3D analysis and relatively close to measured data. Other researchers (e.g., Bergado and Long 1994; Huang et al. 2009) also have obtained good results using the 2D equivalent area approach to model the behavior of embankments and MSE walls supported by soil improved using discrete columns, such as aggregate piers. Zhang et al. (2014) have shown that factors of safety determined using the 2D equivalent area method correspond well with the results of 3D finite element analyses. The 2D simplification is also typically justified because 3D modeling is much more time consuming and requires significantly more modeling expertise (Ariyaratne et al. 2013). The finite element analyses (FEA) used by this study incorporated the equivalent area or panel method.

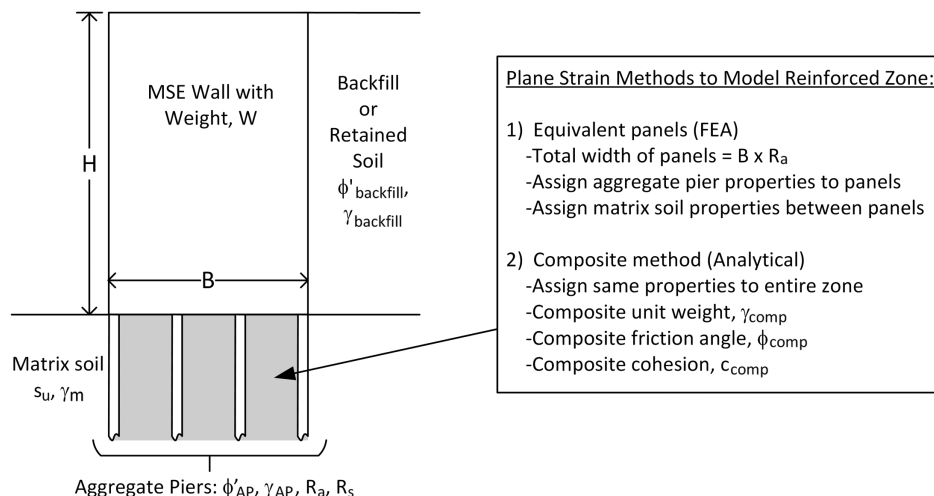


Fig. 2. Modeling an MSE wall supported by an AP improved foundation.

For limit equilibrium problems, the effect of the AP on the soil properties is often considered using a set of composite shear strength parameters, ϕ_{comp} and c_{comp} , and a composite unit weight, γ_{comp} . This approach allows the area replacement ratio to be considered and the difference in stiffness between the AP and the matrix soil. Assuming a saturated, undrained matrix soil ($\phi'_m = 0$, $s_{u,m}$) and cohesionless aggregate piers, the composite unit weight, and cohesion intercept for the AP zone are calculated as (FHWA 1983):

$$\gamma_{comp} = \gamma_{AP}R_a + \gamma_m(1 - R_a) \quad (3)$$

$$c_{comp} = (1 - R_a)s_{u,m} \quad (4)$$

The stiffer response of the AP concentrates the stress from the supported load, allowing the stronger AP to contribute more to the frictional resistance of the AP zone. The stress concentration ratio, R_s , is defined as the vertical stress in the AP divided by the vertical stress in the matrix soil at the same depth. Following Mitchell (1981) and GeoPier (2016), the composite friction angle accounting for stress concentration can be calculated as

$$\phi_{comp} = \tan^{-1} \left(\frac{R_s R_a \tan \phi'_{AP}}{R_a R_s - R_a + 1} \right) \quad (5)$$

Measured values of R_s typically range from 2 to 5 near the top of the pier for flexible structures (Mitchell 1981; HITEC 2007; White et al. 2007; Thompson et al. 2009). The effect of stress concentration can be directly incorporated in the analytical method presented herein.

In situations with relatively low $s_{u,m}$ and/or R_a , the composite shear strength method may not be applicable because of considerations regarding lateral squeeze (e.g., Murugesan and Rajagopal 2006; FHWA 2009; Murugesan and Rajagopal 2010). In those cases, the global stability approach described herein may be inappropriate.

The bearing capacity and FEA employed in this study use perfectly plastic constitutive theory, either implicitly or directly. Under this assumption, the full shear strength can be developed in all soils at the same time. This assumption may not always be true, especially for soft foundation soils that may require higher strain to reach peak strength than the stiffer AP elements. Strain compatibility between the shear strength parameters can be considered by multiplying the peak undrained shear strength of the matrix soil

by a compatibility factor, $\lambda \leq 1$ (Bathurst et al. 2012). This factor could be selected based on the shear stress sustained by the matrix soil at a strain corresponding to the peak strength of the AP. Values of $s_{u,m}$ in this paper can be assumed to include this λ factor.

$$\phi_{comp,mob} = \tan^{-1} \left(\frac{\tan \phi_{comp}}{F_{global}} \right) \quad (6a)$$

$$c_{comp,mob} = \frac{c_{comp}}{F_{global}} \quad (6b)$$

Mobilized Bearing Capacity

The stresses imposed on the foundation by the wall were calculated from the weight of the MSE zone and the active pressure of the backfill. The Coulomb method was used with an interface friction angle of $0.75 \times \phi'_{backfill}$. The horizontal resultant P_{ah} was assumed to act $0.4H$ above the base of the MSE zone (Barker et al. 1991), whereas P_{av} was assumed to act along the back of the MSE. Moments on the MSE zone were used to determine eccentricity.

Definition of Factor of Safety

Bearing capacity solutions are well-developed and familiar to geotechnical engineers. However, as indicated in Fig. 1, they are typically used to calculate a factor of safety in terms of bearing pressure, F_{BC} . In contrast, the factor of safety in terms of shear strength, F_{global} , is commonly used for global stability analysis. Because of nonlinearities introduced by the frictional component of bearing capacity, these two definitions of factor of safety are only equivalent to one another at incipient failure ($F = 1$) or for problems involving only saturated, undrained materials ($\phi_u = 0$).

The difference in these two definitions of factor of safety can be resolved by formulating the global stability problem in terms of mobilized shear strength. For the AP composite zone, the shear strength parameters, ϕ_{comp} and c_{comp} , are divided by the factor of safety as:

A solution is then found by varying the global factor of safety until the sum of the mobilized shear strength along a failure surface is equal to the shear stress required for static equilibrium. In other words, the global factor of safety is found as the value at which the mobilized capacity is equal to the applied stress. This is the approach used by most limit equilibrium slope stability procedures (Duncan et al. 2014).

The same concept can be used in conjunction with bearing capacity theory to determine the global factor of safety for a given foundation bearing pressure, $q_{applied}$. The shear strength parameters for all the soils involved in the analysis can be factored using an approach similar to Eq. (6). Bearing capacity factors are determined for the mobilized shear strength parameters, and the mobilized bearing capacity (MBC), q_{mob} , is calculated. By iteration of F_{global} , the critical factor of safety can be found that results in q_{mob} equal to $q_{applied}$. Because of soil loads from a retained fill, the applied load at the base of a wall will also change as the global factor of safety changes.

The global factors of safety determined using mobilized bearing capacity will differ from those engineers are accustomed to encountering for foundations. To understand the typical relationship between F_{BC} and F_{global} , both were calculated for a symmetrically loaded, continuous foundation with different soil shear strength parameters. These are simpler conditions than those encountered in MSE foundations but provide a useful sense of the relationship between F_{BC} and F_{global} . The results of this comparison are

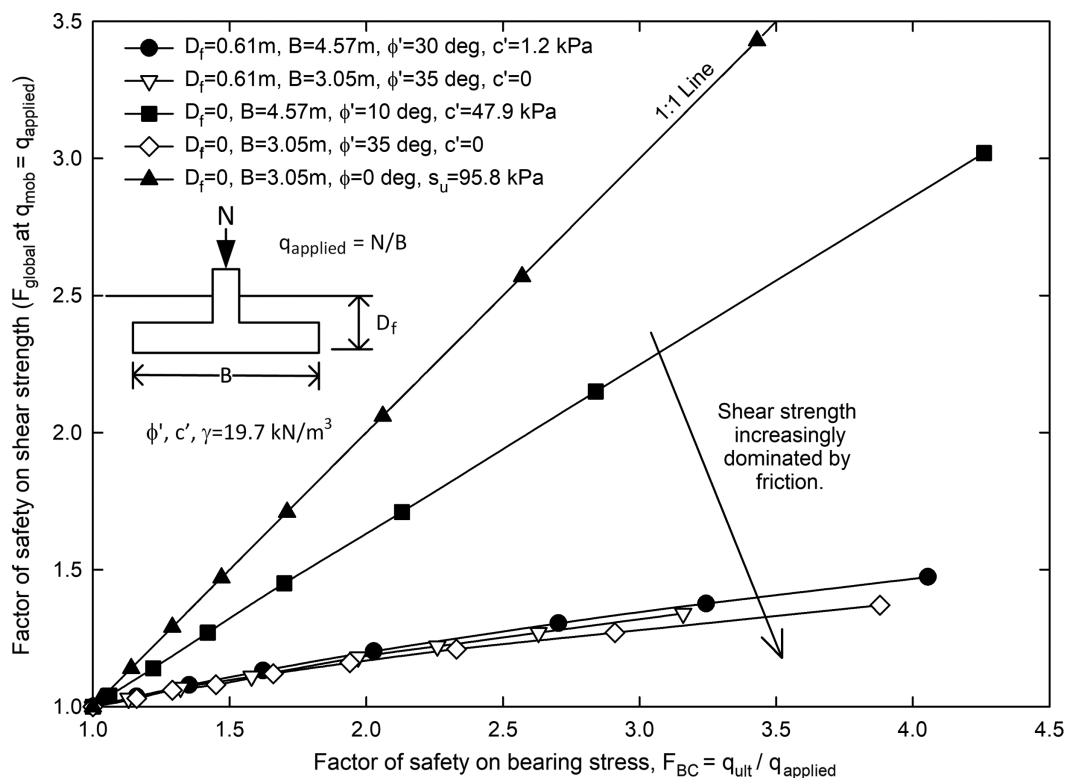


Fig. 3. Correspondence between definitions of factor of safety.

provided in Fig. 3. For cases where the soil is predominantly frictional, a global factor of safety of about 1.5 is equivalent to an F_{BC} of at least 3.5. For soil with a large c' , the value of F_{BC} becomes much closer to F_{global} . The two factors of safety will be equal for undrained ($\phi_u = 0$) conditions.

Failure Surface Shape for Inclined Loading

In the remainder of this paper, the mobilized bearing capacity approach is applied to the design of MSE walls on foundations improved with aggregate piers. The iterative design process uses trial values of F_{global} and can be solved by a trial-and-error approach or with a spreadsheet-based solver. A flowchart of the design process is available in Fig. S1.

The bearing capacity of the soil below the MSE wall depends on the resistance along a critical failure surface. For foundations improved with aggregate piers, this surface passes through both the AP zone (Regions I and II in Fig. 4(a)) and the matrix soil (Regions III and IV). Referring to Fig. 4, the idealized stress state is constant throughout Region I and throughout Region IV but different in each of these regions. In Region I, the stress on the horizontal plane is equal to the applied stress at the base of the wall ($q_{applied}, \tau_{applied}$). In addition, the Mohr circle for Region I must pass through the applied stress and intersect the mobilized composite failure envelope [Fig. 4(b)]. These two constraints are sufficient to define the angle of the mobilized failure surface with respect to horizontal, θ , as shown in Fig. 4(a) and the dimension, R_0 . The major principal stress in Region IV is horizontal, and the inclination of the mobilized failure surface for Region IV, β , is equal to $45^\circ + \phi'/2$ or 45° for $\phi_u = 0$. Regions II and III represent the centered fan associated with reorientation of the stress system (e.g., Davis and Selvadurai 2002) and are defined by a logarithmic spiral in the AP zone and a circular arc within the matrix soil. The mobilized failure surface defined in this manner can be determined by finding a value of θ that satisfies the conditions in Fig. 4(b) (see Fig. S2 for guidance on this calculation).

Because the failure surface passes through two zones with distinctly different shear strength parameters, the contribution of each zone to the overall bearing capacity must be considered. Referring to Eq. (1), the N_c term is strongly influenced by the length of the failure surface relative to the width of the load, whereas the N_γ term represents the work performed on the weight of soil above the failure surface (Davis and Selvadurai 2002). The N_q term has not been considered herein because the walls in this study are assumed to have no embedment. Temporarily assuming all the soil has composite properties, approximate bearing capacity weighting factors for the AP zone below the wall can be defined as:

$$p_{c,AP} \approx \frac{L_I + L_{II}}{L_I + L_{II} + L_{III} + L_{IV}} = \frac{k_2 \cot \theta + \exp(\theta k_1) - 1}{k_2 \cot \theta + \exp(\eta k_1)(1 + k_2) - 1} \quad (7a)$$

$$p_{\gamma,AP} \approx \frac{A_I + A_{II}}{A_I + A_{II} + A_{III} + A_{IV}} = \frac{2k_1 \cot \theta + \exp(2\theta k_1) - 1}{2k_1 \cot \theta + \exp(2\eta k_1)(1 + 4k_1 \sin \beta \cos \beta) - 1} \quad (7b)$$

where $p_{c,AP}$ = weighting factor applied to the N_c term, $p_{\gamma,AP}$ = weighting factor applied to the N_γ term, and L_i = lengths along the failure surface (Fig. 4), A_i = cross-sectional areas (proportional to weight), $k_1 = \tan(\phi_{comp,mob})$, $k_2 = \sin(\phi_{comp,mob})$, θ = inclination of the failure surface below the wall, η = angle of the centered fan (equal to $45 - \phi'_{comp,mob}/2$), and β = inclination of the passive wedge below horizontal. The weighting factors calculated in Eq. (7) reduce the bearing capacity of the AP zone to include capacity only from the portion of the failure surface that lies within the AP zone. When calculating the bearing capacity of the AP zone, the $p_{c,AP}$ factor is multiplied in the N_c term in Eq. (1). Likewise, the $p_{\gamma,AP}$ factor is multiplied in the N_γ term.

Similarly, temporarily assuming homogeneous matrix soil below the wall, the contribution of the bearing capacity weighting factor for the matrix soil contribution can be found as

$$p_{c,m} \approx \frac{L_{III} + L_{IV}}{L_I + L_{II} + L_{III} + L_{IV}} = \frac{\frac{\pi}{4} + 1}{\cot \theta + \frac{\pi}{4} + \theta + 1} \quad (8)$$

Derivations of Eqs. (7) and (8) are provided in Figs. S3 and S4. The factors are plotted in Fig. 5. Eq. (8) reduces the bearing capacity contributed by the matrix soil by half for the condition of no inclined load ($\theta = 45^\circ$). Further reduction in $p_{c,m}$ occurs as the applied pressure α increases, θ decreases, and less of the failure surface passes through the soil adjacent to the AP zone. The $p_{c,m}$ factor is multiplied in the N_c term in the calculation of bearing capacity for the matrix zone.

The weighting factors assume that the vertical boundary of the AP zone coincides with the face of the MSE wall, which is a common design assumption. If the AP zone extends significantly beyond the face of the wall, these factors will underestimate the available mobilized bearing capacity.

The bearing capacity factors in Eqs. (7)–(8) are multiplied along with the other bearing capacity factors in Eq. (1) to determine the contributions of the matrix soil and the AP zone to the overall bearing capacity, which becomes:

$$q_{mob} = q_{mob,AP} + q_{mob,m} \quad (9)$$

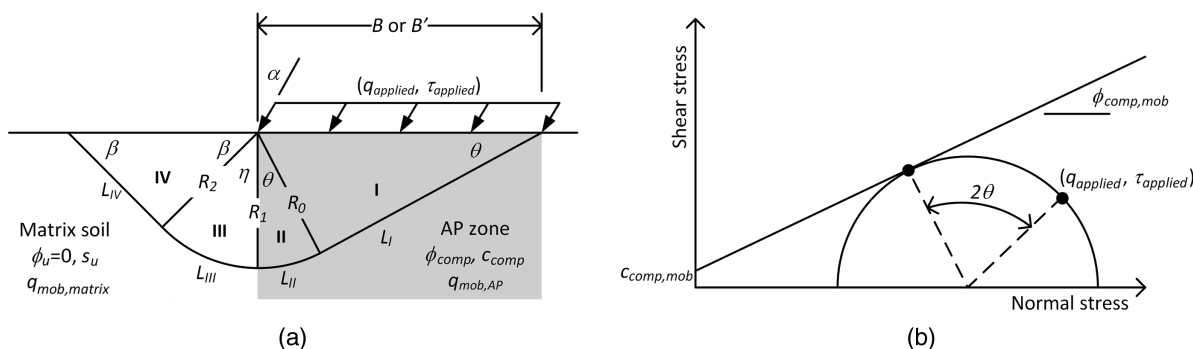


Fig. 4. Definition of the failure surface below the inclined MSE wall load: (a) failure surface; and (b) stress state in Region I.

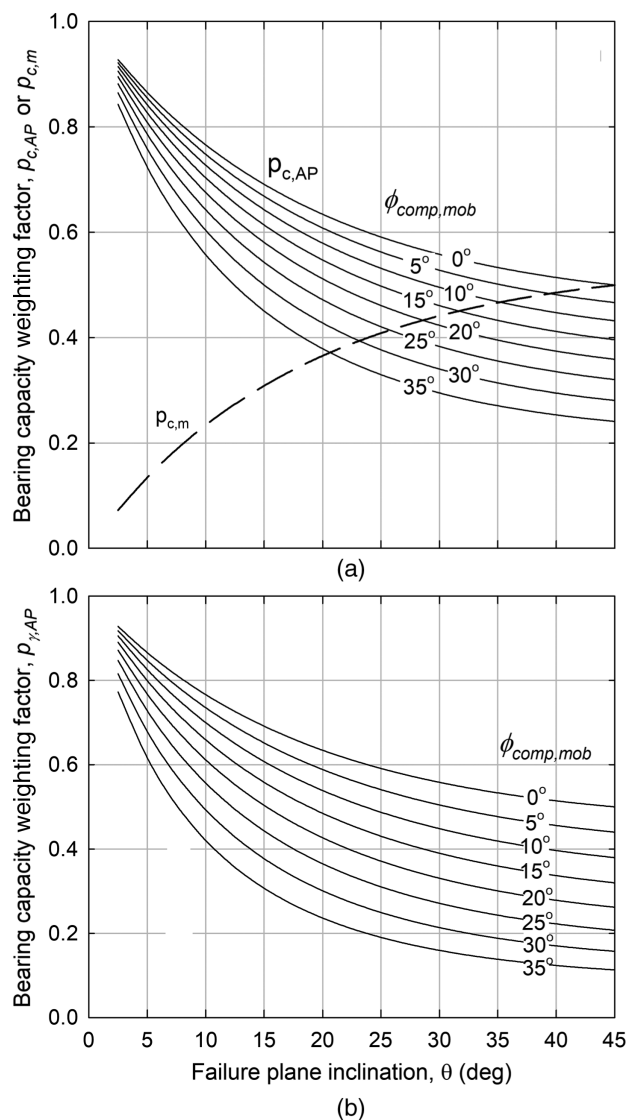


Fig. 5. Bearing capacity weighting factors for foundation with matrix and AP zones: (a) weighting factors applied to N_c term; and (b) weighting factors applied to N_γ term.

where $q_{mob,AP}$ = mobilized bearing capacity of the AP zone, and $q_{mob,m}$ = mobilized bearing capacity of the matrix soil calculated using mobilized shear strength parameters. Summation of the contributions of the bearing capacities for the AP and matrix zones is appropriate because the capacities have been reduced to account for the problem geometry and load inclination. For example, in the case of no inclined load ($\theta = 45^\circ$) and no AP ($\phi'_{comp} = 0$), both $p_{c,m}$ and $p_{c,AP} = 0.5$, and Eq. (9) yields the Meyerhof solution for undrained conditions and homogeneous soil.

Comparative Finite Element Analyses

Finite Element Simulations

2D FE simulations of MSE retaining walls supported on an AP improved zone in a clay matrix soil were created in RS2 (Rocscience) by Reed (2018). The foundation soil and AP panels were initialized under gravity loading. The MSE zone and retained backfill were subsequently placed in the simulations in 10 layers of equal thickness because initial stresses and deformations can be

dependent on the method of *constructing* the model (Kulhawy 1969). While staged FE modeling is not always used for strength reduction analysis and is not necessarily required, staging was used in this case to represent the construction process more accurately. The wall heights considered were 6.10 and 15.2 m with widths of 4.27 and 10.7 m, respectively. Area replacement ratios of the AP ranged from 5% to 30% (FHWA 2017). Each geometry was analyzed for a range of undrained strengths for the matrix soil. The MSE and AP panels were assigned an effective friction angle of 45° , whereas $\phi' = 30^\circ$ (chosen as conservative lower bound) was used for the retained fill. The MSE zone was modeled as elastic to prevent failure of the vertical face and to simplify the analysis, assuming that the MSE reinforcement (not modeled) would prevent yielding in this zone. All the other soils were modeled as elastic-perfect plastic. The elastic moduli of the matrix soil, backfill, and AP were assumed to be $100 \times s_{u,m}$ (Duncan and Buchiagnani 1987), 47.9, and 144 MPa, respectively. The study did not investigate failure through the MSE zone so the modeling did not include the geosynthetic reinforcement or the facing. Further details on the finite element modeling procedure used can be found in Reed and VandenBerge (2019).

The factor of safety, F_{FEA} , was found for the finite element simulations using the strength reduction method. After the simulations reached full height, the shear strength parameters for all the soils except the MSE zone were divided by a strength reduction factor [same process as Eq. (6)], and the simulation was reanalyzed. F_{FEA} was assumed equal to the critical strength reduction factor, which is the largest factor at which the simulation remains marginally stable and converges to a solution.

The failure surface shape from a FE strength reduction analysis can be evaluated by examining the location of high shear strains in the simulation. The results of one simulation are shown in Fig. 6. The analytically determined failure surfaces through the AP zone and matrix soil are shown for cases where eccentricity is ignored (solid line) and where eccentricity is considered (dotted line). A clearly defined active failure surface develops in the retained backfill and along the backside of the MSE zone. Similarly, an angled zone of high shear strain occurs below the wall, aligning with the bottom of Region I. Some of the highest shear strains occur in the toe of the wall and within the centered fan (Regions II and III). The high shear strain in these regions is associated with the reorientation of the stress system. Farther from the toe (Region IV), the maximum shear strain is lower, and the major principal stress is essentially horizontal.

Stress Concentration

The mobilized bearing capacity method uses the area replacement ratio, R_a , and the stress concentration ratio, R_s , to calculate the composite shear strength parameters. Whereas the area replacement ratio is selected as part of the design, the stress concentration ratio must be estimated based on the relative stiffness of the AP and matrix soil and experience.

The FE simulation results were used to determine R_s at the condition of fully mobilized shear strength (i.e., critical strength reduction factor). As plotted in Fig. 7, the FE simulations did not show significant variation in R_s as a function of R_a . At a given R_a , the scatter in R_s is related to tendencies for R_s to decrease as the matrix soil became stiffer and to increase as the wall height increased. The plotted values of R_s from the FE simulations are average values for the four AP trenches based on stresses extracted from the upper few meters of the AP zone. Eccentricity of loading caused more stress concentration in the AP trench below the toe of the wall and

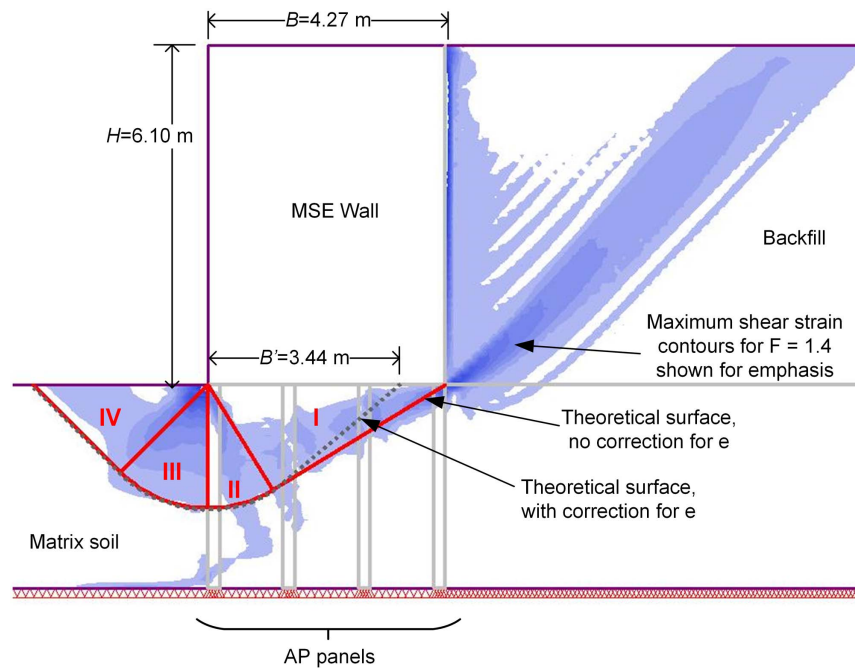


Fig. 6. Contours of maximum shear strain (dark = high strain) from strength reduction analysis on a wall with $s_{u,m} = 36$ kPa, $R_a = 0.2$, and $F_{FEA} = 1.3$.

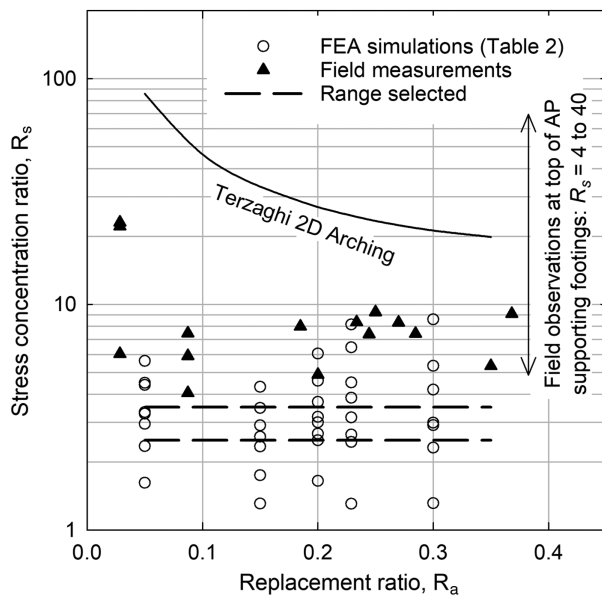


Fig. 7. Comparison of stress concentration ratios from FEA simulations and field measurements by others. (Data from Lawton and Fox 1994; White et al. 2007; Thompson et al. 2009; Sloan 2011; Briançon and Simon 2012.)

significantly less stress concentration below the heel. For comparison, R_s values are plotted for 2D Terzaghi arching theory and field measurements below footings (Lawton and Fox 1994; White et al. 2007) and embankments (Thompson et al. 2009; Chen et al. 2010; Sloan 2011; Briançon and Simon 2012; Filz et al. 2019). Whereas measurements of R_s tend to be in the range of 4–40 for rigid foundations supported by AP, HITEC (2007) recommends using a value in the range of 2–5 for stability applications for flexible structures, such as MSE walls. The effect of R_s on the mobilized bearing

capacity approach will be evaluated by using constant value of R_s of either 2.5 or 3.5 and the R_s values extracted from the FE simulations.

Comparison of Analytical and FEA Results

Mobilized bearing capacity and FEA simulations were calculated for 39 combinations of wall geometry, AP replacement ratio, and foundation soil undrained shear strength, which are summarized in Table 2. The geometries resulted in eccentricity to MSE wall width (e/B) ratios of 0.04–0.15, indicating reduced widths that were between 92% and 70% of the full MSE wall width. The load inclinations ranged from 7.5° to 18.7° with six cases close to or more than 15° for which the Meyerhof inclination factors may not be appropriate (Ukrichron et al. 1998). The mobilized bearing capacity calculations were performed in four different ways: (1) ignore effects of stress concentration and eccentricity, (2) use $R_s = 2.5$ and ignore eccentricity, (3) use $R_s = 2.5$ and the reduced width, B' , to correct for eccentricity, and (4) use $R_s = 3.5$ and correct for eccentricity. The factors of safety calculated in each manner are provided in Table 2. To evaluate the suitability of the MBC approach, the factors of safety are compared with the results of the FE strength reduction analyses in Fig. 8.

When both the stress concentration ratio and eccentricity are ignored, the mobilized bearing capacity method predicted nearly the same factor of safety as FEA for F between 1 and 1.5 as indicated in Fig. 8(a). The factor of safety from the MBC approach was on average about 4% lower than the FE results. The largest differences between the factors of safety for the two methods occurred for F below 1.0 and above 1.5. In the MBC analyses, ignoring the eccentricity correction tends to increase F while neglecting the stiffness ratio tends to decrease F . Although a relatively good match is found between the two methods in Fig. 8(a), a more robust approach that does not rely on offsetting errors is preferred.

To assess the influence of the stiffness factor, the mobilized bearing capacity method was used with R_s of 2.5 and ignoring

Table 2. Factors of safety from mobilized bearing capacity and finite element approaches

Geometry	$s_{u,m}$ (kPa)	Load inclination, α^a (degrees)	Mobilized bearing capacity approach				F_{FEA}
			F_{global}	F_{global}	F_{global}	F_{global}	
			$R_s = 1$ (Full B)	$R_s = 2.5$ (Full B)	$R_s = 2.5$ (Use B')	$R_s = 3.5$ (Use B')	
H = 6.10 m	24	8.8	0.91	0.9	0.84	0.87	0.89
B = 4.27 m	36	11.4	1.22	1.22	1.08	1.11	1.16
$R_a = 5\%$	48	13.3	1.51	1.52	1.29	1.32	1.36
	72	16.1	2.01	2.11	1.65	1.68	1.75
H = 6.10 m	48	14.2	1.46	1.59	1.37	1.42	1.5
B = 4.27 m	68	16.4	1.94	2.05	1.66	1.71	1.9
$R_a = 15\%$	96	18.5	2.44	2.68	2.01	2.06	2.24
H = 6.10 m	24	11	0.91	1.08	1	1.07	1.02
B = 4.27 m	36	12.9	1.19	1.36	1.21	1.27	1.3
$R_a = 20\%$	48	14.5	1.46	1.62	1.4	1.46	1.46
	72	16.9	2.42	2.14	1.73	1.79	1.85
H = 6.10 m	12	8.9	0.62	0.84	0.8	0.88	0.85
B = 4.27 m	24	11.3	0.92	1.11	1.02	1.1	1.06
$R_a = 22.9\%$	48	14.7	1.46	1.64	1.41	1.48	1.5
	96	18.7	2.41	2.74	2.02	2.08	2.2
H = 6.10 m	12	9.8	0.68	0.93	0.87	0.96	0.86
B = 4.27 m	24	11.8	0.95	1.18	1.08	1.16	1.06
$R_a = 30\%$	48	14.9	1.46	1.67	1.44	1.51	1.55
	96	18.7	2.38	2.64	2.02	2.08	2.26
H = 15.2 m	48	7.5	0.72	0.77	0.73	0.76	0.86
B = 10.7 m	72	9.9	0.99	1.04	0.94	0.97	0.995
$R_a = 5\%$	84	10.9	1.12	1.16	1.04	1.06	1.1
	96	11.8	1.24	1.28	1.13	1.15	1.2
H = 15.2 m	48	9.4	0.76	0.91	0.85	0.92	0.87
B = 10.7 m	72	11.3	1.01	1.14	1.04	1.1	1.08
$R_a = 15\%$	84	12.1	1.13	1.26	1.13	1.19	1.19
	96	12.9	1.24	1.37	1.21	1.27	1.28
H = 15.2 m	48	10.1	0.79	0.97	0.91	0.98	0.9
B = 10.7 m	72	11.8	1.02	1.19	1.08	1.15	1.14
$R_a = 20\%$	84	12.6	1.14	1.3	1.17	1.23	1.21
	96	13.3	1.25	1.41	1.25	1.31	1.32
H = 15.2 m	48	10.4	0.8	1	0.94	1.01	0.9
B = 10.7 m	72	12.1	1.03	1.22	1.11	1.18	1.16
$R_a = 22.9\%$	84	12.8	1.15	1.33	1.19	1.26	1.25
	96	13.5	1.25	1.43	1.26	1.33	1.35
H = 15.2 m	48	11.1	0.85	1.08	1	1.08	0.9
B = 10.7 m	72	12.6	1.06	1.28	1.16	1.23	1.2
$R_a = 30\%$	84	13.2	1.16	1.38	1.23	1.3	1.31
	96	13.8	1.27	1.48	1.3	1.37	1.37

^a α corresponds to analyses with $R_s = 3.5$, corrected for eccentricity.

the effects of eccentricity. As shown in Fig. 8(b), the MBC approach predicts higher F when the composite friction angle is adjusted for the stiffness ratio using Eq. (5). Inclusion of the stiffness ratio in the calculations increased F_{global} by an average of about 27%, and the values of F_{global} are an average of 20% higher than F_{FEA} when eccentricity is ignored. The inclusion of R_s also removes scatter from the prediction of F_{global} as evidenced by increased linearity in the trend in Fig. 8(b).

The final two analysis cases considered both the stiffness ratio and the eccentricity correction in the mobilized bearing capacity calculation. As shown in Figs. 8(c and d), the relationship between F_{global} and F_{FEA} is quite linear for factors of safety above 1. With R_s of 2.5, the MBC approach tended to underpredict F with an error up to about -10%. When R_s is increased to 3.5, the MBC approach fits the FEA results very well, especially if the analyses with high values of α and F less than one are ignored (average error = 0%, standard deviation = 5%).

Scatter occurs for systems with high and low F because the failure mechanism diverges from a mode analogous to bearing capacity. Factors of safety near or less than unity tend to occur when the

matrix soil is weak and soft. A stability number for the matrix soil, N_m , can be defined as

$$N_m = \frac{\gamma_t H}{s_{u,m}} \quad (10)$$

where γ_t = total unit weight of the backfill, H = height of the MSE wall, and $s_{u,m}$ = the undrained shear strength of the matrix soil, including strain compatibility correction.

The variation in F_{FEA} with N_m is plotted in Fig. 9. A transition in the general trend occurs when N_m exceeds a value of about 5. The FEAs with high N_m predict downward movement of the entire backfill zone and horizontal sliding of the improved zone and MSE wall, similar to lateral squeezing. The mobilized bearing capacity approach should not be expected to predict accurate factors of safety consistently for these cases.

The six models had high values of α , which indicate a high ratio between the horizontal and vertical load applied at the base of the MSE wall. As noted by Ukritchon et al. (1998), Meyerhof's correction is excessive for high α , which explains why F_{global} is lower

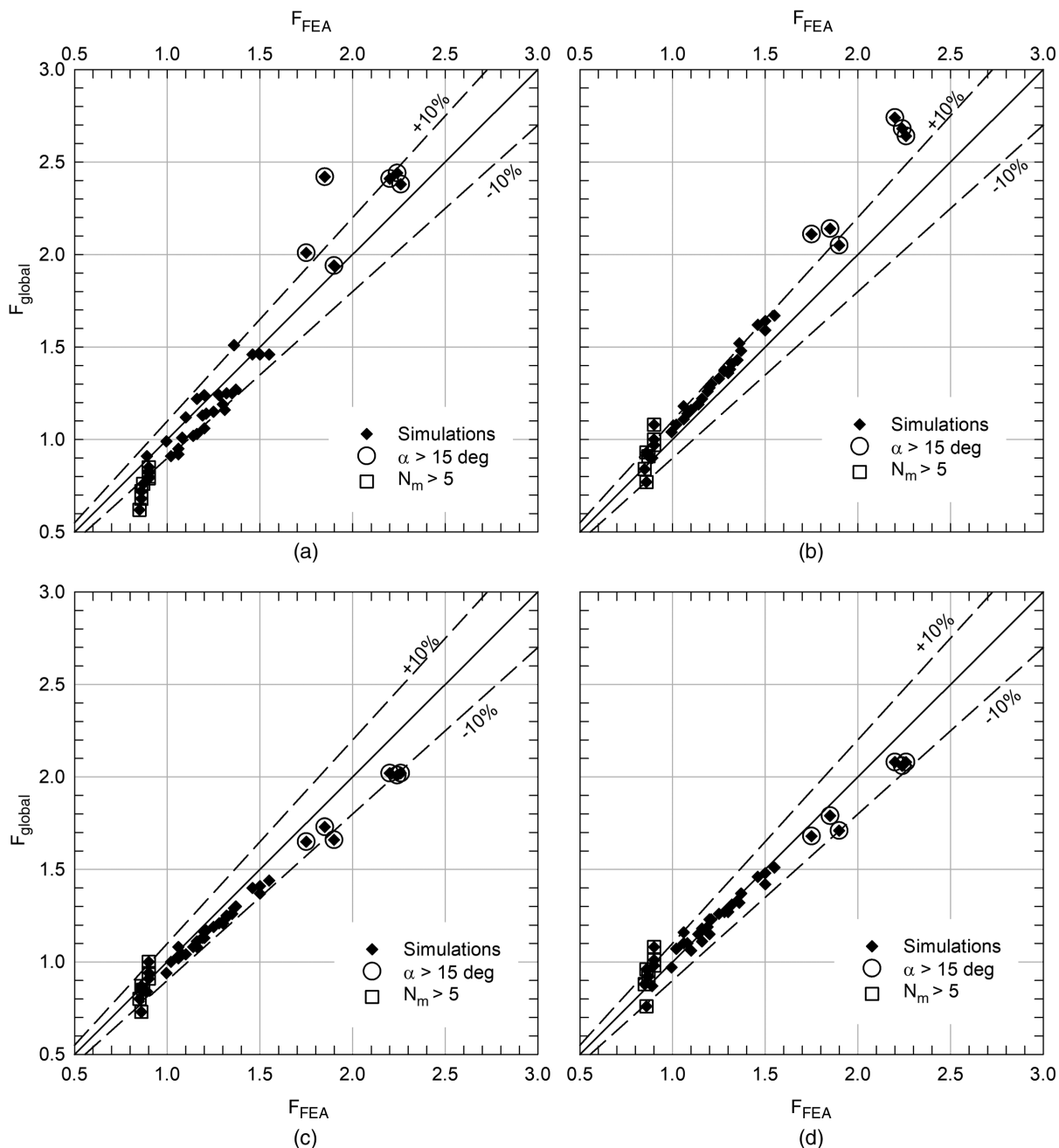


Fig. 8. Comparison of factors of safety from mobilized bearing capacity and FEA: (a) $R_s = 1$, ignore eccentricity; (b) $R_s = 2.5$, ignore eccentricity; (c) $R_s = 2.5$, with eccentricity correction; and (d) $R_s = 3.5$, with eccentricity correction.

than F_{FEA} for these cases. However, the general trend between F_{global} and F_{FEA} remains consistent for these analyses.

As indicated in Fig. 7, the FE simulations produced average values of R_s between 1.3 and 8.6. The highest values of R_s occurred when the matrix soil was weak and soft as expected. To further understand the effect of R_s on the MBC method, the average R_s from each FE simulation was used in the MBC approach to calculate F_{global} . The ratios of F_{global} to F_{FEA} are plotted in Fig. 10 with respect to N_m for different values of R_s . Where the average R_s was less than 3.5, the MBC approach predicted a ratio less than or equal to 1, which is conservative. For low values of N_m and FEA R_s , the MBC approach predicted a lower stability than the FE simulations. This conservative error appears to be the result of eccentricity and either the method used to find a single value of R_s from the FE

simulations or the Meyerhof correction factors. Further exploration of these effects would be needed to understand this more fully. When N_m was greater than 4, the FE simulation R_s values were greater than 3.5. In these cases, the MBC method was largely unconservative if the FEA R_s was used. However, as indicated in Fig. 9, lateral squeezing is indicated for N_m greater than 5. To limit unconservative estimates of the factor of safety, a cap of 3.5 is proposed on the R_s value used with the MBC approach and aggregate piers. The results for constant R_s of 3.5 are also plotted in Fig. 10, and the MBC approach produces F_{global} generally less than or equal to F_{FEA} with the exception of cases with N_m approaching 5.

The relationship between the global factor of safety and the bearing stress-based factor of safety as illustrated in Fig. 3 must be kept in mind when interpreting the results of this study.

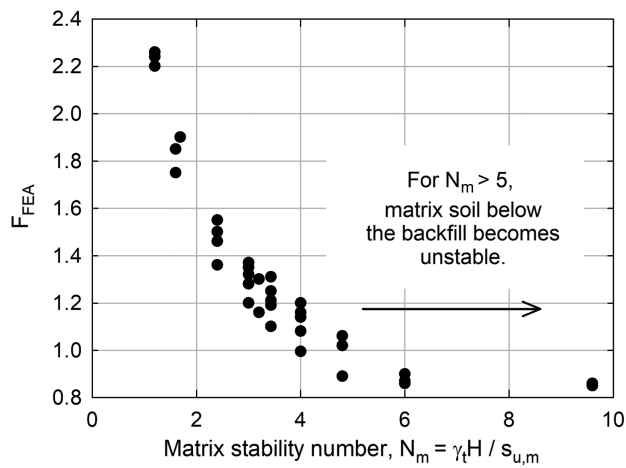


Fig. 9. Variation of factor of safety with matrix soil stability number, N_m .

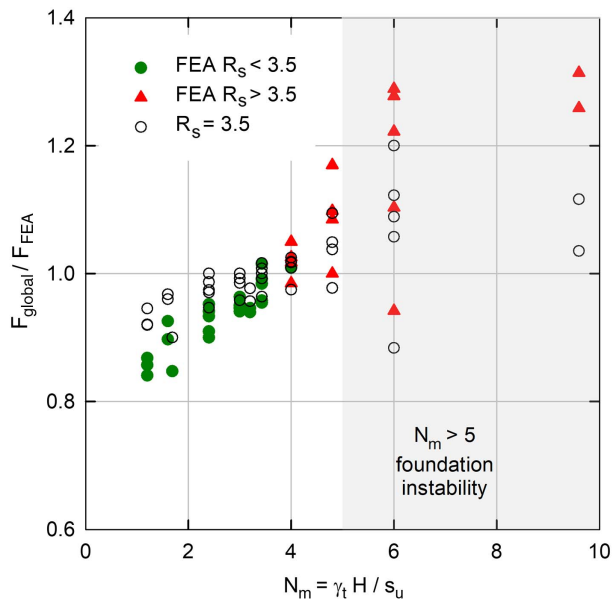


Fig. 10. Ratio of F_{global} to F_{FEA} compared with N_m for different values of R_s .

For reference, F_{BC} was calculated for each of the MSE walls analyzed using the assigned shear strengths. The combined ultimate bearing capacity was calculated using Eqs. (7)–(9) for F_{global} equal to unity. The eccentricity calculated for the ultimate conditions, and $q_{applied}$ was calculated using the corresponding reduced area [Eq. (2)]. The two definitions of factor of safety are compared in Fig. 11 for the MSE walls simulated in this study. As expected, the two definitions are equal at a factor of safety of about 1. At a given F_{global} , the value of F_{BC} increases as the replacement ratio increases and AP zone becomes more frictional, similar to the trends in Fig. 3.

Fig. 11 further illustrates that design for bearing capacity and global stability are interconnected. As F_{global} approaches a typical design factor of safety of 1.5, the bearing capacity factor of safety approaches 3. Thus, for the cases modeled in this paper, satisfaction of one design requirement (i.e., bearing capacity or global stability) implies that the other requirement is also met. Fig. 11 can be used to

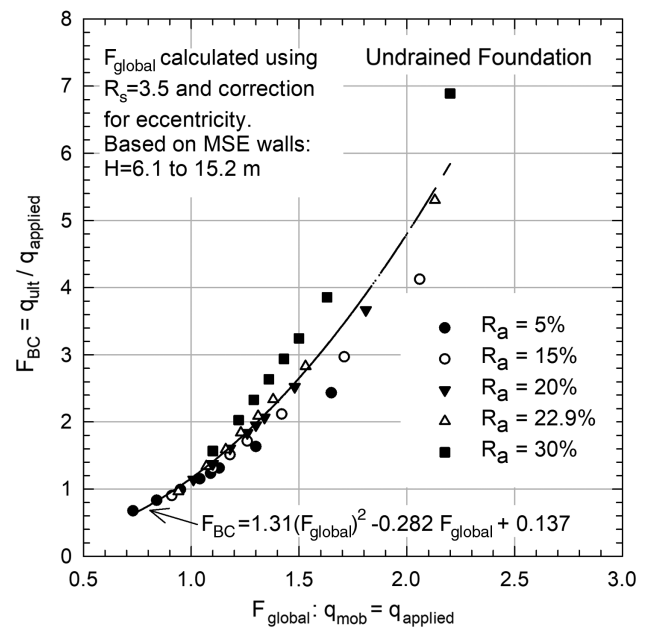


Fig. 11. Relationship of F_{global} to bearing stress-based factor of safety, F_{BC} , for common MSE geometry.

relate calculated global stability to conventional undrained bearing capacity for MSE walls in the range explored by this study.

Design Recommendations and Example

The mobilized bearing capacity approach can be applied to MSE wall design through any analytical tool (e.g., spreadsheet, computer program, electronic engineering notebook) that can perform the iterative calculation illustrated in Fig. S1. Aside from the selection of shear strength parameters and geometry, the design decisions and checks that must be made by the engineer are summarized in Table 3.

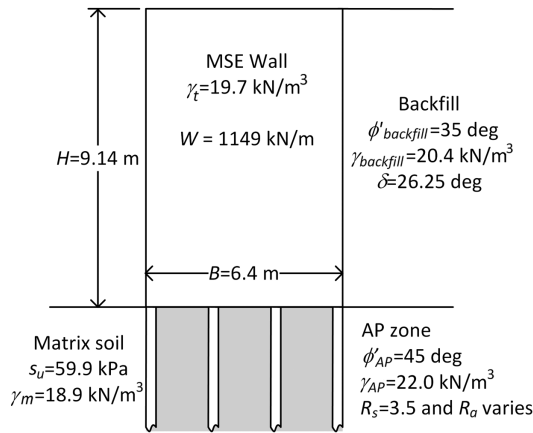
An example MSE wall is shown in Fig. 12 along with a single iteration of the design calculations for an initial value of F_{global} and $R_a = 0.05$. If repeated sufficiently, the calculations in Fig. 11 will converge to a value of $F_{global} = 1.22$. Table 4 summarizes the variation in design parameters for other values of R_a for this example geometry and soil conditions, which would assist the selection of an appropriate R_a for the support of the wall. The recommendations in Table 3 assume that the AP zone is only below the MSE wall, which is a conservative assumption. If additional foundation soil is improved beyond the toe of the wall, the weighting factors used to calculate q_{mob} would need to be adjusted based on the geometry to consider this change.

Conclusions

Bearing capacity and global stability have traditionally been analyzed using different definitions of the factor of safety, the former in terms of bearing stress and the later in terms of shear strength. However, bearing capacity analysis can be reformulated in terms of shear strength through the mobilized bearing capacity concept, similar to the analysis of slopes. The novel MBC approach allows the bearing capacity theory to be connected directly to global stability analysis. The two definitions of factor of safety differ the

Table 3. Design recommendations for application of mobilized bearing capacity to MSE wall design

Design consideration	Recommendation
Include effects of stiffness factor, R_s ?	Yes. Use value in range of 2.5–3.5, or similar value based on prior experience.
Correct for eccentricity?	Yes. Meyerhof reduced area approach is appropriate.
How to determine q_{mob} ?	Use the bearing capacity factors in Eqs. (7) and (8) to correct for failure through two soil zones.
How to determine the magnitude and location of backfill forces, P_{ah} and P_{av} ?	The calculations presented in this paper used the Coulomb method with an interface friction angle of $0.75 \times \phi'_{backfill}$. P_{ah} was assumed to act $0.4H$ above the base of the wall (Barker et al. 1991). P_{av} was assumed to act along the back of the wall.
Is the load inclination angle, α , less than 15° ?	Yes–Meyerhof correction factor is appropriate. No–Meyerhof correction may be incorrect. Sliding behavior will dominate rather than bearing capacity or global stability.
Is the stability number in a suitable range?	N_m should be less than 5, which matches FHWA (2009) guidance for squeezing.



1. Assume $F_{global} = 1.1$ and $R_a = 0.05$
2. Mobilized strength parameters (factor by F_{global})
AP: $\phi'_{comp,mob} = 8^\circ$ (includes $R_s = 3.5$), $c_{comp,mob} = 51.7$ kPa
Matrix: $s_{u,mob} = 54.4$ kPa
Backfill: $\phi'_{backfill,mob} = 32.5^\circ$
3. Backfill loads
 $P_{a-v} = 94.9$ kN/m, $P_{a-h} = 210$ kN/m
4. Eccentricity correction
 $e = 0.37$ m, $B' = 5.66$ m
5. Stress state at base of wall
 $q_{applied} = 220$ kPa, $\tau_{applied} = 37.1$ kPa, $\alpha = 9.6^\circ$, $\theta = 33.8^\circ$
6. Bearing capacity factors
 $\theta = 33.8^\circ$, $p_{c,AP} = 0.49$, $p_{\gamma,AP} = 0.45$, $p_{c,m} = 0.45$
7. Mobilized bearing capacities
 $q_{matrix} = 101$ kPa, $q_{AP} = 152$ kPa
 $q_{mob} = 101 + 152 = 253$ kPa
8. Compare mobilized and applied pressures
 $q_{applied} (= 220 \text{ kPa}) < q_{mob} (= 253 \text{ kPa})$
9. Increase F_{global} and repeat calculations

Fig. 12. MSE wall example with one iteration of design calculations.**Table 4.** Variation of design parameters with R_a for example ($R_s = 3.5$)

R_a	e/B	α (degrees)	q_{mob} (kPa)	F_{global}
0	0.059	9.7	221	1.11
0.05	0.067	10.5	225	1.20
0.10	0.073	11.1	228	1.26
0.20	0.081	11.9	233	1.36
0.30	0.086	12.4	236	1.42

most for materials dominated by friction and are equivalent for soils modeled as purely cohesive.

The shape of the theoretical failure surface within the MSE wall foundation can be approximated by the consideration of the stress states below the wall and beyond the toe. The applied load and mobilized shear strength in the aggregate pier zone control the initial inclination of the failure surface. The calculated failure surfaces match well with the high shear strain zones observed in the FE models. Equations for approximate bearing capacity factors that account for two zones (matrix and AP) separated by a vertical boundary were presented. These factors assume that the boundary of the AP zone coincides with the face of the MSE wall.

The mobilized bearing capacity approach can be used to determine the global stability and/or bearing capacity of MSE walls founded on soil foundations improved with aggregate piers. Compared with the companion FEA, the most accurate results are obtained when the eccentricity correction is used. Whereas the

FE simulations predict higher values of R_s in some cases, a cap of 3.5 is proposed for use with the MBC approach. For F above about 1.5, the MBC approach underpredicts the factor of safety, which may be the result of the Meyerhof load inclination factor for the cases considered. The mobilized bearing capacity approach also may be incorrect for cases with values of N_m greater than 5, especially if the aggregate piers are limited to the zone directly below the MSE wall. Further refinements to the MBC approach could be obtained by evaluating other methods to extract R_s from the FE simulations and/or by comparison with 3D FEA.

This study only considered undrained conditions in the matrix soil and did not consider the possibility of slip surfaces extending through the MSE zone. Engineers using the proposed method must consider the potential impacts of these limitations on their designs.

Data Availability Statement

Some or all data, models, or code that support the findings of this study are available from the corresponding author upon reasonable request.

Acknowledgments

The authors acknowledge GeoPier Foundation Company's financial support of the numerical analyses performed for this study

and collaboration on technical aspects of AP design for MSE wall support. Tennessee Tech's Department of Civil and Environmental Engineering and Center for Energy Systems Research are also acknowledged for their support of the authors. The authors also thank the anonymous reviewers for their valuable contributions and suggestions, which greatly improved this paper.

Supplemental Materials

Figs. S1–S4 are available online in the ASCE Library (www.ascelibrary.org).

References

- Ariyaratne, P., D. S. Liyanapathirana, and C. J. Leo. 2013. "Comparison of different two-dimensional idealizations for a geosynthetic-reinforced pile-supported embankment." *Intl. J. Geomech.* 13 (6): 754–768. [https://doi.org/10.1061/\(ASCE\)GM.1943-5622.0000266](https://doi.org/10.1061/(ASCE)GM.1943-5622.0000266).
- Barker, R. M., J. M. Duncan, K. B. Rojiani, P. S. Ooi, C. K. Tan, and S. G. Kim. 1991. *Manuals for the design of bridge foundations: Shallow foundations, driven piles, retaining walls and abutments, drilled shafts, estimating tolerable movements, and load factor design specifications and commentary*. Washington, DC: Transportation Research Board.
- Bathurst, R. J., K. Hatami, and M. C. Alfaro. 2012. "Geosynthetic-reinforced soil walls and slopes—Seismic aspects." In *Handbook of geosynthetic engineering*, 2nd ed., 317–363. London: ICE Publishing.
- Bergado, D. T., and P. V. Long. 1994. "Numerical analysis of embankment on subsiding ground improved by vertical drains and granular piles." In *Proc. 13th ICSMFE*, 1361–1366. New Delhi, India: Oxford and IBH Publishing.
- Briançon, L., and B. Simon. 2012. "Performance of pile-supported embankment over soft soil: Full-scale experiment." *J. Geotech. Geoenviron. Eng.* 138 (4): 551–561. [https://doi.org/10.1061/\(ASCE\)GT.1943-5606.0000561](https://doi.org/10.1061/(ASCE)GT.1943-5606.0000561).
- Chen, R. P., Z. Z. Xu, Y. M. Chen, D. S. Ling, and B. Zhu. 2010. "Field tests on pile-supported embankments over soft ground." *J. Geotech. Geoenviron. Eng.* 136 (6): 777–785. [https://doi.org/10.1061/\(ASCE\)GT.1943-5606.0000295](https://doi.org/10.1061/(ASCE)GT.1943-5606.0000295).
- Davis, R. O., and A. P. Selvadurai. 2002. *Plasticity and geomechanics*. Cambridge, UK: Cambridge University Press.
- Diaz, C., G. Taylor, and L. Shao. 2012. "Ground improvement under a MSE embankment wall in an urban environment." In *Proc., 4th Int. Conf. Grouting Deep Mixing 2012*. Reston, VA: ASCE. <https://ascelibrary.org/doi/abs/10.1061/9780784412350.0059>.
- Duncan, J. M., and A. L. Buchiagnani. 1987. *Engineering manual for settlement studies*. Blacksburg, VA: Center for Geotechnical Practice and Research.
- Duncan, J. M., S. G. Wright, and T. L. Brandon. 2014. *Soil strength and slope stability*. New York: Wiley.
- FHWA (Federal Highway Administration). 1983. *Design and construction of stone columns—Volume I*. FHWA/RD-83/026. Washington, DC: FHWA.
- FHWA (Federal Highway Administration). 2009. *Design and construction of mechanically stabilized earth walls and reinforced soil slopes—Volume I*. FHWA-NHI-10-024. Washington, DC: FHWA.
- FHWA (Federal Highway Administration). 2016. *Limit equilibrium design framework for MSE structures with extensible reinforcement*. FHWA-HIF-17-004. Washington, DC: FHWA.
- FHWA (Federal Highway Administration). 2017. *Ground modification methods reference manual—Volume I*. FHWA-NHI-16-027. Washington, DC: FHWA.
- Filz, G. M., J. A. Sloan, M. P. McGuire, M. Smith, and J. Collin. 2019. "Settlement and vertical load transfer in column-supported embankments." *J. Geotech. Geoenviron. Eng.* 145 (10): 04019083. [https://doi.org/10.1061/\(ASCE\)GT.1943-5606.0002130](https://doi.org/10.1061/(ASCE)GT.1943-5606.0002130).
- GeoPier Foundation Company. 2016. *GeoPier shear reinforcement for global stability and slope stability*. Davidson, NC: GeoPier Foundation.
- HITEC (Highway Innovative Technology Evaluation Center). 2007. *HITEC evaluation of Geopier rammed aggregate piers*. Reston, VA: ASCE.
- Huang, J., J. Han, and S. Oztoprak. 2009. "Coupled mechanical and hydraulic modeling of geosynthetic-reinforced column-supported embankments." *J. Geotech. Geoenviron. Eng.* 135 (8): 1011–1021. [https://doi.org/10.1061/\(ASCE\)GT.1943-5606.0000026](https://doi.org/10.1061/(ASCE)GT.1943-5606.0000026).
- Hutchinson, D. L. 2011. "Case study of a foundation improvement beneath MSE walls for a highway embankment." In *Geo-Frontiers 2011*. Reston, VA: ASCE. <https://ascelibrary.org/doi/abs/10.1061/41165%28397%29349>.
- Kulhawy, F. H. 1969. "Finite element analysis of the behavior of embankments." Ph.D. dissertation, Univ. of California. <http://oskicat.berkeley.edu/record=b14306556-S1>.
- Lawton, E. C., and N. S. Fox. 1994. "Settlement of structures supported on marginal or inadequate soils stiffened with short aggregate piers." In *Vertical and horizontal deformations of foundations and embankments*, 962–974. Reston, VA: ASCE.
- Leshchinsky, D., and J. Han. 2004. "Geosynthetic reinforced multitiered walls." *J. Geotech. Geoenviron. Eng.* 130 (12): 1225–1235. [https://doi.org/10.1061/\(ASCE\)1090-0241\(2004\)130:12\(1225\)](https://doi.org/10.1061/(ASCE)1090-0241(2004)130:12(1225)).
- Leshchinsky, D., F. Vahedifard, and B. A. Leshchinsky. 2012. "Revisiting bearing capacity analysis of MSE walls." *Geotext. Geomembr.* 34 (Oct): 100–107. <https://doi.org/10.1016/j.geotextmem.2012.05.006>.
- Mankbadi, R., J. Mansfield, R. Wilson-Fahmy, S. Hanna, and V. Krstic. 2004. "Ground improvement utilizing vibro-concrete columns." In *GeoSupport 2004*. Reston, VA: ASCE. <https://ascelibrary.org/doi/abs/10.1061/40713%282004%2955>.
- Meyerhof, G. G. 1963. "Some recent research on the bearing capacity of foundations." *Can. Geotech. J.* 1 (1): 16–26. <https://doi.org/10.1139/t63-003>.
- Mitchell, J. K. 1981. "Soil improvement: State of the art." In *Proc., 10th Int. Conf. Soil Mechanics Foundation Engineering*, 509–565. Rotterdam, Netherlands: A.A. Balkema.
- Murugesan, S., and K. Rajagopal. 2006. "Geosynthetic-encased stone columns: Numerical evaluation." *J. Geotextiles Geomembr.* 24 (6): 349–358. <https://doi.org/10.1016/j.geotextmem.2006.05.001>.
- Murugesan, S., and K. Rajagopal. 2010. "Studies on the behavior of single and group of geosynthetic encased stone columns." *J. Geotech. Geoenviron. Eng.* 136 (1): 129–139. [https://doi.org/10.1061/\(ASCE\)GT.1943-5606.0000187](https://doi.org/10.1061/(ASCE)GT.1943-5606.0000187).
- Reed, E. C. 2018. "Comparison of FEA and analytical methods for determining stability of a RAP supported MSE wall." M.S. thesis, Dept. of Civil Engineering, Tennessee Technological Univ.
- Reed, E. C., and D. R. VandenBerge. 2019. "Comparison of FEA and analytical methods for determining stability of a RAP supported MSE wall." *J. Deep Found. Inst.* 12 (2): 122–129. <https://doi.org/10.1080/19375247.2018.1562593>.
- Sloan, J. A. 2011. "Column-supported embankments: Full-scale tests and design recommendations." Ph.D. dissertation, Dept. of Civil and Environmental Engineering, Virginia Tech.
- Sloan, S. W. 2013. "Geotechnical stability analysis." *Géotechnique* 63 (7): 531–571. <https://doi.org/10.1680/geot.12.RL.001>.
- Spencer, E. 1967. "A method of analysis of the stability of embankments assuming parallel inter-slice forces." *Géotechnique* 17 (1): 11–26. <https://doi.org/10.1680/geot.1967.17.1.11>.
- Stuedlein, A. W., M. Bailey, D. Lindquist, J. Sankey, and W. J. Neely. 2010. "Design and performance of a 46-m-high MSE wall." *J. Geotech. Geoenviron. Eng.* 136 (6): 786–796. [https://doi.org/10.1061/\(ASCE\)GT.1943-5606.0000294](https://doi.org/10.1061/(ASCE)GT.1943-5606.0000294).
- Thompson, M. J., K. J. Wissmann, and H. T. Pham. 2009. "Performance monitoring of a rammed aggregate pier foundation supporting a mechanically stabilized earth wall." *J. Perform. Constr. Facil.* 23 (4): 244–250. [https://doi.org/10.1061/\(ASCE\)CF.1943-5509.0000010](https://doi.org/10.1061/(ASCE)CF.1943-5509.0000010).
- Ukritchon, B., A. J. Whittle, and S. W. Sloan. 1998. "Undrained limit analyses for combined loading of strip footings on clay." *J. Geotech. Geoenviron. Eng.* 124 (3): 265–276. [https://doi.org/10.1061/\(ASCE\)1090-0241\(1998\)124:3\(265\)](https://doi.org/10.1061/(ASCE)1090-0241(1998)124:3(265)).
- VandenBerge, D. R. 2017. "V-shaped failure surfaces in bearing capacity type limit equilibrium analysis." In *GeoFrontiers 2017*. Reston, VA: ASCE. <https://ascelibrary.org/doi/abs/10.1061/9780784480458.001>.

White, D. J., H. T. V. Pham, and K. K. Hoelkamp. 2007. "Support mechanisms of rammed aggregate piers. I: Experimental results." *J. Geotech. Geoenviron. Eng.* 133 (12): 1503–1511. [https://doi.org/10.1061/\(ASCE\)1090-0241\(2007\)133:12\(1503\)](https://doi.org/10.1061/(ASCE)1090-0241(2007)133:12(1503)).

Zhang, Z., J. Han, and G. Ye. 2014. "Numerical investigation on factors for deep-seated slope stability of stone column-supported embankments over soft clay." *Eng. Geology* 168 (Jan): 104–113. <https://doi.org/10.1016/j.enggeo.2013.11.004>.